arXiv:1512.05285v1 [math.NA] 16 Dec 2015

ANALYSIS OF A NEW HARMONICALLY ENRICHED MULTISCALE COARSE SPACE FOR DOMAIN DECOMPOSITION METHODS

MARTIN J. GANDER, ATLE LONELAND, AND TALAL RAHMAN

Abstract. We propose a new, harmonically enriched multiscale coarse space (HEM) for domain decomposition methods. For a coercive high contrast model problem, we show how to enrich the coarse space so that the method is robust against any variations and discontinuities in the problem parameters both inside subdomains and across and along subdomain boundaries. We prove our results for an enrichment strategy based on solving simple, lower dimensional eigenvalue problems on the interfaces between subdomains, and we call the resulting coarse space the spectral harmonically enriched multiscale coarse space (SHEM). We then also give a variant that performs equally well in practice, and does not require the solve of eigenvalue problems, which we call non-spectral harmonically enriched multiscale coarse space (NSHEM). Our enrichment process naturally reaches the optimal coarse space represented by the full discrete harmonic space, which enables us to turn the method into a direct solver (OHEM). We also extensively test our new coarse spaces numerically, and the results confirm our analysis

1. Introduction

It is well known that domain decomposition methods which are based on local communication between subdomains need the addition of a coarse problem in order to be scalable, see for example the books [27, 29] and references therein. The coarse space components of the coarse problem can however do much more than just make a method scalable: work and difficulties of the underlying domain decomposition method can be transferred into the coarse space, and an optimal coarse space can even make the underlying domain decomposition method into a direct solver [13, 14], like optimal transmission conditions based on the Dirichlet to Neumann operator can make a Schwarz method into a direct solver, see [11, 21] and references therein for optimal Schwarz methods, and [15] for transmission conditions which include an optimal coarse space component that leads to convergence in two iterations, independently of the number of subdomain and underlying equation. Such optimal transmission conditions and coarse space components are however very expensive to use, and in practice one approximates them. In the case of transmission conditions, this led to the new class of optimized Schwarz methods, which have the same computational cost per iteration as classical Schwarz methods, but converge much faster; for an overview and references, see [11]. In the case of coarse spaces, one can select the most important subspace of the optimal coarse space to increase the performance of the method, an example of this has been shown in [14].

We present here a simple procedure that allows us to systematically enrich a given coarse space, up to a maximum degree where it becomes a direct solver. Since our interest is in high contrast problems, we start with a classical multiscale finite element coarse space. The multiscale finite element method was developed to cope with problems that have many spatial

Key words and phrases. Domain Decomposition, Multiscale Coarse Space, Harmonic Enrichment, Two-level methods, Problems with large coefficient variation.

$\delta = 2h$	$\delta = 4h$	$\delta = 6h$	$\delta = 8h$	$\delta = 10h$	$\delta = 12h$	$\delta = 14h$	$\delta = 16h$
610(3.6e6)	339(1.1e6)	330(7.1e5)	241(3.5e5)	224(2.9e5)	222(2.5e5)	33(3.4e1)	30(2.8e1)

TABLE 1. Iteration and condition number estimate for the distribution in Figure 1 for a classical two level additive Schwarz method when increasing the overlap δ, with $h = \frac{1}{128}$, $H = 16h$ and contrast $\alpha = 10^6$.

scales [18]. The idea is to replace the classical finite element shape functions by harmonic functions, i.e. functions that solve the underlying equation locally. An important problem in multiscale finite element methods is what boundary conditions one should impose on these harmonic shape functions. The approach we propose here for our coarse space enrichment can also be used to enrich a multiscale finite element space, and if combined with non-overlapping subdomain solves, will in the limit reach the fine scale finite element solution, which is an important property of our enrichment process.

Domain decomposition methods for problems where the discontinuities in the coefficient are resolved by the coarse mesh and the subdomains have been analyzed thoroughly, (cf. [2, 5,6,20,25,31] and references therein). In the case where the discontinuous coefficients are not aligned with the coarse mesh or the underlying subdomains, efforts have been made to develop coarse spaces that would ultimately lead to robust methods with respect to the contrast in the problems. We mention especially the use of coarse spaces consisting of multiscale finite element basis functions introduced in [18]. This approach was first studied in [1] and later analyzed in [17], where the precise dependence of two level Schwarz methods on the high contrast in a problem was given for the specific case of isolated inclusions. Also, the importance of harmonic shape functions was shown for coarse grid corrections. A finite volume multiscale coarse space was proposed in [22] and in [23, 24] FETI methods were analyzed for multiscale problems.

A first idea to enrich the coarse space by eigenfunctions for tackling problems with high contrast can be found in [9, 10], where selected subdomain eigenfunctions are combined with different types of partition of unity functions and the importance of the initial coarse space based on multiscale and energy minimizing basis functions is discussed, see also [7]. A different way to construct a coarse space using eigenfunctions of the Dirichlet to Neumann map of each subdomain was proposed in [4]. This approach was later improved by solving a generalized eigenvalue problem in the overlaps [28]. A good overview of the most recent approaches can be found in [26].

We start with a numerical experiment to motivate our new harmonic enrichment process. The problem configuration is shown in Figure 1. We show in Table 1 the iteration numbers and condition number estimates for a two level additive Schwarz method when increasing the overlap, where the coarse space is the multiscale coarse space introduced in [17]. We see that initially increasing the overlap improves the method, but increasing further does not help much, until we reach the overlap $\delta = 14h$, where a substantial improvement happens. Why is this so? Looking at Figure 1, we see that there are many highly conductive channels across the interfaces, which means that an error component will travel with very little damping across these channels. Following the original maximum principle argument of Schwarz, the error will thus not diminish substantially, until the overlap includes the entire channel, at which point rapid convergence will set in. This is a typical case where the underlying domain decomposition method has difficulties, and these difficulties can be transferred into the coarse

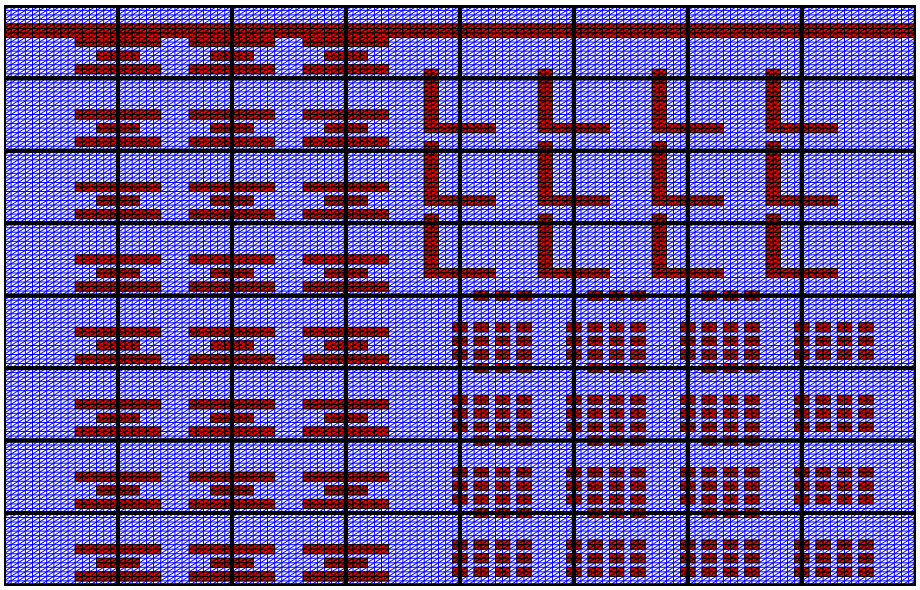

FIGURE 1. Distribution of α for a geometry with $h = \frac{1}{128}$, $H = 16h$. The regions marked with red are where α has a large value.

space. The present multiscale coarse space is however not good enough to handle these difficulties.

The purpose of our manuscript is to show how one can systematically transfer such a difficulty into the coarse space by enriching it with well chosen harmonic functions to obtain a harmonically enriched multiscale coarse space (HEM), and to prove that with HEM the method is then robust with respect to the coefficient jumps. In order to prove our results, we need to base the enrichment on an eigenvalue problem on the interfaces between the subdomains, which leads to the spectral harmonically enriched multiscale coarse space (SHEM). For SHEM, we have to solve lower dimensional eigenvalue problems in the construction phase. Because they are lower dimensional however, our construction process is much cheaper than the construction based on volume subdomain eigenvalue problems, Dirichlet to Neumann eigenvalue problems or generalized eigenvalue problems in the overlap. We then show numerically that one can obtain an equally good harmonic enrichment without eigenvalue problems, which we call the non-spectral harmonically enriched multiscale coarse space (NSHEM).

2. PRELIMINARIES

2.1. **The Model Problem.** We consider as our model problem the elliptic boundary value problem

$$\begin{aligned} -\nabla \cdot (\alpha(x)\nabla u) &= f \qquad \text{in } \Omega, \\ u &= 0 \qquad \text{on } \partial\Omega, \end{aligned} \tag{1}$$

where Ω is a bounded convex domain in $\mathbb{R}^2$, $f \in L^2(\Omega)$ and $\alpha \in L^\infty(\Omega)$ with the property that $\alpha \geq \alpha_0$ for some positive constant α_0.

The weak formulation of (1) is: find $u \in H_0^1(\Omega)$ such that

$$a(u,v) = \int_\Omega f v \, dx \quad \forall v \in H_0^1(\Omega), \tag{2}$$

where

$$a(u,v) = \int_\Omega \alpha(x) \nabla u \cdot \nabla v \, dx.$$

We discretize (2) with standard P_1 finite elements on a mesh $\mathcal{T}_h$ of Ω such that

$$\overline{\Omega} = \bigcup_{K \in \mathcal{T}_h} K,$$

where the finite element space is defined as

$$V_h^0(\Omega) := \{v \in C_0(\Omega) : v|_K \in P_1(K)\}.$$

The discrete problem corresponding to (2) is: find $u_h \in V_h^0(\Omega)$ such that

$$a(u_h,v) = \int_\Omega f v \, dx \quad \forall v \in V_h^0(\Omega). \tag{3}$$

Without loss of generality we will assume that the coefficient α is piecewise constant over each element K, i.e.,

$$\alpha(x) = \alpha_K \text{ for all } x \in K.$$

We also introduce the following notation: for positive constants c and C independent of the mesh parameters h, H, the overlap δ (which we will define below) and the coefficient α, we define $u \simeq v$, $x \succeq y$ and $w \preceq z$ as

$$cu \leq v \leq Cu, \qquad x \geq cy \qquad \text{and} \qquad w \leq Cz.$$

Here, u, v, x, y, w and z denote norms of some functions.

2.2. **Subdomains.** Let Ω be partitioned into non-overlapping open, connected Lipschitz polytopes $\{\Omega_i : i = 1, \ldots, N\}$ such that $\overline{\Omega} = \bigcup_{i=1}^N \overline{\Omega}_i$, where each $\overline{\Omega}_i$ is assumed to consist of elements from $\mathcal{T}_h(\Omega)$. We assume that this partitioning is shape-regular. By extending each subdomain Ω_i with a distance δ in each direction, we create a further decomposition of Ω into overlapping subdomains $\{\Omega_i'\}_{i=1}^N$. We consider here only the specific case of small overlap $\delta = 2h$, but a slight modification of the proof will also cover the case of minimal overlap h. We denote the layer of elements in Ω_i touching the boundary $\partial\Omega_i$ by Ω_i^h and assume that the triangles corresponding to this layer are shape regular and define the minimum diameter of these triangles as $h_i := \min_{K \in \mathcal{T}_h(\Omega_i^h)} h_K$, where h_K is the diameter of the triangle K. We define the interface between two subdomains to be the open edge shared by the subdomains, i.e., $\overline{\Gamma}_{ij} := \overline{\Omega}_i \cap \overline{\Omega}_j$. The sets of vertices of elements in $\mathcal{T}_h(\Omega)$ (nodal points) belonging to Ω, Ω_i, $\partial\Omega$, $\partial\Omega_i$ and Γ_{ij} are denoted by Ω_h, Ω_{ih}, $\partial\Omega_h$, $\partial\Omega_{ih}$ and Γ_{ijh}. With each interface we define the space of finite element functions restricted to Γ_{ij} and zero on $\partial\Gamma_{ij}$ as $V_h^0(\Gamma_{ij})$.

The weighted L^2-inner product and the corresponding weighted L^2-norm is defined as

$$(u,v)_{L^2_\alpha(G)} := (\alpha(x)u, v)_{L^2(G)} \qquad \text{and} \qquad \|u\|^2_{L^2_\alpha(G)} := (u,u)_{L^2_\alpha(G)},$$

where G is some domain contained in Ω.

We define the restriction of the bilinear form $a(\cdot,\cdot)$ to an interface, $\Gamma_{ij} \subset \Gamma$, shared by two subdomains as

$$a_{\Gamma_{ij}}(u,v) := \left(\alpha_{|\Gamma_{ij}}(x) D_{x^t} u, D_{x^t} v\right)_{L^2(\Gamma_{ij})},$$

where $\alpha_{|\Gamma_{ij}}(x) := \lim_{y \in \Omega_i \to x} \alpha(y)$ and D_{x^t} denotes the tangent derivative with respect to Γ_{ij}. In order to obtain continuous basis functions across subdomain interfaces, we define a second bilinear form on each interface Γ_{ij},

$$\bar{a}_{\Gamma_{ij}}(u,v) := (\overline{\alpha}_{ij}(x) D_{x^t} u, D_{x^t} v)_{L^2(\Gamma_{ij})},$$

where $\overline{\alpha}_{ij}$ is taken as the maximum of $\alpha_{|\Gamma_{ij}}$ and $\alpha_{|\Gamma_{ji}}$. An evident, but important relation following directly from this definition is that

$$\bar{a}_{\Gamma_{ij}}(u,v) \simeq a_{\Gamma_{ij}}(u,v) + a_{\Gamma_{ji}}(u,v). \tag{4}$$

The geometric domain decomposition induces a decomposition of $V_h^0(\Omega)$ into local subspaces: for each Ω_i', the corresponding local subspace is

$$V_i := \left\{ v \in V_h^0(\Omega) \,:\, \mathrm{supp}(v) \subset \Omega_i' \right\}.$$

This yields a decomposition of $V_h^0(\Omega)$,

$$V_h^0(\Omega) = V_0 + \sum_{i=1}^{N} V_i,$$

where the coarse space, V_0, is a special space which we will define later. For $i = 0, \ldots, N$ we define the projection like operators $T_i \colon V_h^0(\Omega) \to V_i$ as

$$a(T_i u, v) := a(u,v) \qquad \forall v \in V_i, \tag{5}$$

and introduce the operator

$$T := T_0 + T_1 + \cdots + T_N. \tag{6}$$

This allows us to replace the original problem (3) by the equation

$$Tu = g, \tag{7}$$

where $g = \sum_{i=0}^{N} g_i$ and $g_i = T_i u$. Note that g_i can be computed without knowing the solution u of (3).

2.3. **Eigenvalue Problems on Interfaces.** The first new harmonic enrichment of our coarse space is based on solutions of local eigenvalue problems along the interfaces between subdomains:

Definition 2.1 (Generalized Eigenvalue Problem)**.** *For each interface $\Gamma_{ij} \subset \Gamma$, we define the generalized eigenvalue problem: Find ψ and λ, such that*

$$\bar{a}_{\Gamma_{ij}}(\psi, v) := \lambda b_{\Gamma_{ij}}(\psi, v) \qquad \forall v \in V_h^0(\Gamma_{ij}), \tag{8}$$

where $b_{\Gamma_{ij}}(\psi, v) := h_i^{-1} \sum_{k \in \Gamma_{ijh}} \beta_k \psi_k v_k$ *and* $\beta_k = \sum_{\substack{K \in \mathcal{T}_h(\Omega) \\ k \in \mathrm{dof}(K)}} \alpha_K$.

The following lemma is a slight modification of Lemma 2.11 in [28] and provides important estimates for the eigenfunction projection.

Lemma 2.2. *Define* $M := \dim(V_h^0(\Gamma_{ij}))$ *and let the eigenpairs* $\{(\psi^k_{\Gamma_{ij}}, \lambda^k_{ij})\}_{k=1}^{\dim(V_h^0(\Gamma_{ij}))}$ *of the generalized eigenvalue problem (8) be ordered such that*

$$0 < \lambda^1_{ij} \leq \lambda^2_{ij} \ldots \leq \lambda^M_{ij} \quad \textit{and} \quad b_{\Gamma_{ij}}(\psi^k_{\Gamma_{ij}}, \psi^l_{\Gamma_{ij}}) = \delta_{kl} \quad \textit{for any} \quad 1 \leq k, l \leq M.$$

Then, the projection for any integer $0 \leq m_{ij} \leq M$

$$\Pi_{\mathrm{m}} v := \sum_{k=1}^{m_{ij}} b_{\Gamma_{ij}}(v, \psi^k_{\Gamma_{ij}}) \psi^k_{\Gamma_{ij}}$$

is a-orthogonal, and therefore

$$|\Pi_{\mathrm{m}} v|_{\bar{a}_{\Gamma_{ij}}} \leq |v|_{\bar{a}_{\Gamma_{ij}}} \quad \textit{and} \quad |v - \Pi_{\mathrm{m}} v|_{\bar{a}_{\Gamma_{ij}}} \leq |v|_{\bar{a}_{\Gamma_{ij}}}, \qquad \forall v \in V_h^0(\Gamma_{ij}). \tag{9}$$

In addition we also have the approximation estimate

$$\|v - \Pi_{\mathrm{m}} v\|^2_{b_{\Gamma_{ij}}} \leq \frac{1}{\lambda^{m_{ij}+1}_{ij}} |v - \Pi_{\mathrm{m}} v|^2_{\bar{a}_{\Gamma_{ij}}}, \qquad \forall v \in V_h^0(\Gamma_{ij}). \tag{10}$$

Proof. Following the lines of the proof given in [28, Lemma 2.11], we start out by recognizing that since both $\bar{a}_{\Gamma_{ij}}$ and $b_{\Gamma_{ij}}$ are positive definite, we may reduce the generalized eigenvalue problem to a standard eigenvalue problem, where standard spectral theory guarantees the existence of eigenpairs $\{(\psi^k_{\Gamma_{ij}}, \lambda^k_{ij})\}_{k=1}^{\dim(V_h^0(\Gamma_{ij}))}$, for which the eigenvalues $\{\lambda^k_{ij}\}_{k=1}^{\dim(V_h^0(\Gamma_{ij}))}$ are positive. In addition, we may choose the eigenvectors such that they form a basis of $V_h^0(\Gamma_{ij})$ and satisfy the orthogonality conditions

$$\bar{a}_{\Gamma_{ij}}(\psi^k_{\Gamma_{ij}}, \psi^l_{\Gamma_{ij}}) = b_{\Gamma_{ij}}(\psi^k_{\Gamma_{ij}}, \psi^l_{\Gamma_{ij}}) = 0 \quad \forall k \neq l, \quad |\psi^k_{\Gamma_{ij}}|^2_{\bar{a}_{\Gamma_{ij}}} = \lambda^k_{ij} \text{ and } \|\psi^k_{\Gamma_{ij}}\|^2_{b_{\Gamma_{ij}}} = 1.$$

Now, any $v \in V_h^0(\Gamma_{ij}))$ may be expressed as

$$v = \sum_{k=1}^{\dim(V_h^0(\Gamma_{ij}))} b_{\Gamma_{ij}}(v, \psi^k_{\Gamma_{ij}}) \psi^k_{\Gamma_{ij}}.$$

The $\bar{a}_{\Gamma_{ij}}$-orthogonality states that

$$\left| \sum b_{\Gamma_{ij}}(v, \psi^k_{\Gamma_{ij}}) \psi^k_{\Gamma_{ij}} \right|^2_{\bar{a}_{\Gamma_{ij}}} = \sum b_{\Gamma_{ij}}(v, \psi^k_{\Gamma_{ij}})^2 \left| \psi^k_{\Gamma_{ij}} \right|^2_{\bar{a}_{\Gamma_{ij}}}.$$

From this we have

$$|v|^2_{\bar{a}_{\Gamma_{ij}}} = |\Pi_{\mathrm{m}} v|^2_{\bar{a}_{\Gamma_{ij}}} + |v - \Pi_{\mathrm{m}} v|^2_{\bar{a}_{\Gamma_{ij}}},$$

and (9) follows directly. To prove (10), we start by using the $b_{\Gamma_{ij}}$ - orthonormality of the eigenfunctions

$$\begin{aligned}
\|v-\Pi_{\mathrm{m}}v\|^2_{b_{\Gamma_{ij}}} &= \left\| \sum_{k=m_{ij}+1}^{\dim(V_h^0(\Gamma_{ij}))} b_{\Gamma_{ij}}(v,\psi^k_{\Gamma_{ij}})\psi^k_{\Gamma_{ij}} \right\|^2_{b_{\Gamma_{ij}}} \\
&= \sum_{k=m_{ij}+1}^{\dim(V_h^0(\Gamma_{ij}))} b_{\Gamma_{ij}}(v,\psi^k_{\Gamma_{ij}})^2 \frac{1}{\lambda^k_{ij}} |\psi^k_{\Gamma_{ij}}|^2_{\bar{a}_{\Gamma_{ij}}} \\
&\leq \frac{1}{\lambda^{m_{ij}+1}_{ij}} \sum_{k=m_{ij}+1}^{\dim(V_h^0(\Gamma_{ij}))} b_{\Gamma_{ij}}(v,\psi^k_{\Gamma_{ij}})^2 |\psi^k_{\Gamma_{ij}}|^2_{\bar{a}_{\Gamma_{ij}}} \\
&= \frac{1}{\lambda^{m_{ij}+1}_{ij}} |v-\Pi_{\mathrm{m}}v|^2_{\bar{a}_{\Gamma_{ij}}}.
\end{aligned}$$

In the last steps we used the fact that $|\psi^k_{\Gamma_{ij}}|^2_{\bar{a}_{\Gamma_{ij}}} = \lambda^k_{ij}$, that the eigenvalues are ordered in increasing order and that the eigenfunctions are $\bar{a}_{\Gamma_{ij}}$-orthogonal. □

3. Construction of the Coarse Space

In this section we define the coarse space for our method. The coarse space is a multiscale finite element space enriched with harmonic functions based on the generalized eigenvalue problem (8) defined on each interface shared by two subdomains. In order to explain the construction in detail, we start by introducing discrete harmonic functions before we describe how the coarse space is constructed.

3.1. **Discrete Harmonic Functions.**

For each non-overlapping subdomain Ω_i we define the restriction of V_h to $\bar{\Omega}_i$ as

$$V_h(\Omega_i) := \left\{ v_{|\bar{\Omega}_i} : v \in V_h \right\},$$

and the corresponding subspace with zero Dirichlet boundary conditions as

$$V_h^0(\Omega_i) := \{ v \in V_h(\Omega_i) : v(x) = 0 \quad \text{for} \quad x \in \partial\Omega_{ih} \}.$$

Clearly $V_h^0(\Omega_i) \subset V_h(\Omega_i)$. Now let $\mathcal{P}_i : V_h(\Omega_i) \to V_h^0(\Omega_i)$ be the a-orthogonal projection of a function $u \in V_h$ onto $V_h^0(\Omega_i)$ defined by

$$a_i(\mathcal{P}_i u, v) := a_i(u,v) \qquad \forall v \in V_h^0(\Omega_i), \tag{11}$$

and define $\mathcal{H}_i u := u - \mathcal{P}_i u$ as the discrete harmonic counterpart of u, i.e.

$$a_i(\mathcal{H}_i u, v) = 0 \qquad \forall v \in V_h^0(\Omega_i), \tag{12}$$

$$\mathcal{H}_i u(x) = u(x) \qquad x \in \partial\Omega_{ih}. \tag{13}$$

A function $u \in V_h(\Omega_i)$ is locally discrete harmonic if $\mathcal{H}_i u = u$. If all restrictions to subdomains of a function $u \in V_h$ are locally discrete harmonics, i.e.,

$$u_{|\Omega_i} = \mathcal{H}_i u_{|\Omega_i} \qquad \text{for } i = 1, \ldots, N,$$

then we say u is a discrete harmonic function. For any function $u \in V_h$, this gives a decomposition of u into discrete harmonic parts and local projections, i.e. $u = \mathcal{H}u + \mathcal{P}u$.

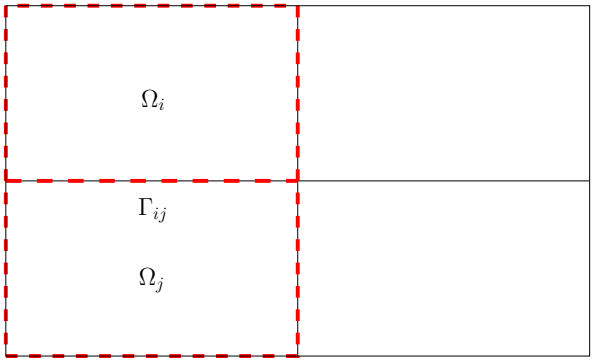

FIGURE 2. Support of a spectral basis function $p^k_{\Gamma_{ij}}$ corresponding to the interface Γ_{ij}.

With the operator $\mathcal{H}$, we can introduce the space of discrete harmonic functions as

$$\tilde{V}_h = \mathcal{H}V_h = \{u \in V_h^0(\Omega) : u_{|\Omega_i} = \mathcal{H}_i u_{|\Omega_i}\}.$$

For a two level method that considers a non-overlapping partitioning of Ω as subdomains, this space is the optimal coarse space. We will in the following sections show how one can approximate this space in a systematic manner by carefully including into the coarse space the most important components of $\tilde{V}_h$ not already included in our initial multiscale finite element coarse space. In the limit, these enrichment strategies will reach the optimal coarse space (OHEM) $\tilde{V}_h$, and allow us to turn the method into a direct solver. This is an important property of our strategy.

With this in mind, we are now ready to define the coarse basis functions.

3.2. **Multiscale Basis Functions.** The multiscale finite element coarse space, which we will consider as our initial coarse space for our method, consists of vertex based discrete harmonic functions associated with each vertex of the polytope Ω_i. More formally, for each vertex x^k of the polytope Ω_i and for each internal edge $\Gamma_{ij} \subset \Omega_i$ that touches x^k, we solve the 1D boundary value problem

$$\begin{aligned} \bar{a}_{\Gamma_{ij}}(\phi^{ms}_{ik}, v) &= 0 \quad \forall v \in V_h^0(\Gamma_{ij}), && \text{(interface values)} \\ \phi^{ms}_{ik}(x^k) &= 1 \quad \text{at the vertex } x^k \text{ of } \Omega_i, \\ \phi^{ms}_{ik} &= 0 \quad \text{at the other vertex.} \end{aligned}$$

Then we extend ϕ^{ms}_{ik} inside Ω_i using the values of ϕ^{ms}_{ik} as boundary conditions on the edges touching x^k and zero on the remaining edges

$$\begin{aligned} a_i(\phi^{ms}_{ik}, v) &= 0 \quad \forall v \in V_h^0(\Omega_i), && \text{(harmonic extension inside)} \\ \phi^{ms}_{ik}(x) &= 0 \quad x \in \partial\Omega_i \setminus \Gamma_{ij}, \quad x^k \in \partial\Gamma_{ij}. \end{aligned} \tag{14}$$

The solutions corresponding to each k are then glued together in a natural manner to form multiscale hat functions and extended with zero to the rest of Ω.

3.3. **Spectral Basis Functions.** Let $\psi^k_{\Gamma_{ij}}$ be the k-th eigenfunction of the generalized eigenvalue problem (8) on each interface Γ_{ij}. We then define the spectral basis functions associated

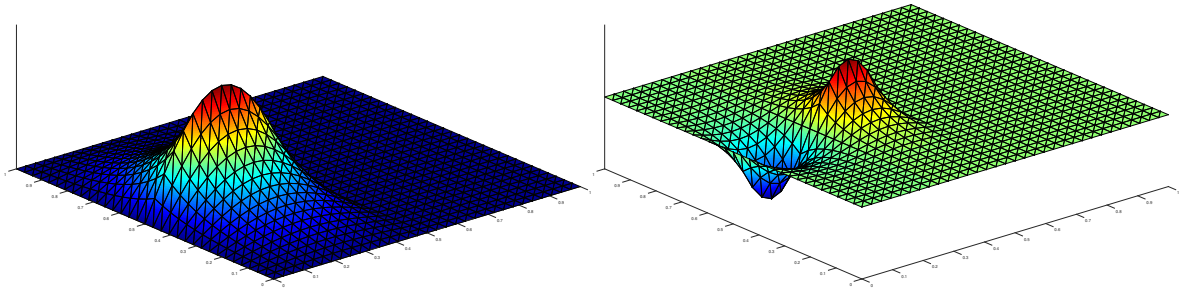

FIGURE 3. Plot of the spectral basis functions for $h = 1/32$ and $H = 16h$. *Left:* first order spectral basis functions. *Right:* second order spectral basis functions.

with the interface Γ_{ij} as the discrete harmonic extension of each of the eigenfunctions $\psi^k_{\Gamma_{ij}}$

$$\begin{aligned} a_i(p^k_{\Gamma_{ij}}, v) &= 0 \qquad && \forall v \in V_h^0(\Omega_i), \\ p^k_{\Gamma_{ij}} &= \psi^k_{\Gamma_{ij}} && x \in \Gamma_{ij}, \\ p^k_{\Gamma_{ij}} &= 0 && x \in (\partial\Omega_i \cup \partial\Omega_j) \setminus \Gamma_{ij}. \end{aligned} \tag{15}$$

Each solution is then extended with zero to the rest of Ω in order to make the functions global.

The spectral harmonically enriched multiscale coarse space (SHEM) is then defined as the span of these two sets of basis functions,

$$V_0 := \text{span}\{\{\phi^{ms}_k\}_{k=1}^{n_\nu} \cup \{\{p^l_{\Gamma_{ij}}\}_{l=1}^{m_{ij}}\}_{\Gamma_{ij}\subset\Gamma}\}. \tag{16}$$

An example of the first and second order spectral basis function is given in Figure 3 for a problem with $\alpha = 1$ and mesh parameters $H = 1/2$ and $h = 1/32$.

4. Analysis of the Preconditioner

In this section we define a suitable interpolation operator into the SHEM coarse space V_0 and provide the necessary bounds for the operator in order to apply the classical abstract Schwarz framework. The aforementioned interpolation operator is a composition of the standard multiscale interpolation operator and a new interpolation operator for the spectral basis functions.

The multiscale interpolation operator is defined as

$$I_{\text{ms}} u := \sum_{k=1}^{n_\nu} u(x^k)\phi^{\text{ms}}_k, \tag{17}$$

where n_ν is the number of internal vertices, i.e. vertices of the polytope Ω_i which are not on $\partial\Omega$. The spectral interpolation operator is defined as

$$\Pi_{\text{m}} u := \sum_{\Gamma_{ij}\subset\Gamma} \sum_{k=1}^{m_{ij}} b_{\Gamma_{ij}}(u_{\Gamma_{ij}}, p^k_{\Gamma_{ij}}) p^k_{\Gamma_{ij}}. \tag{18}$$

Combining these two, the new coarse space interpolation operator $I_0 \colon V_h^0(\Omega) \to V_0$ is defined as

$$I_0 u := I_{\mathrm{ms}} u + \Pi_{\mathrm{m}} \left(u - I_{\mathrm{ms}} u \right). \tag{19}$$

Lemma 4.1 (Stable Decomposition)**.** *For all $u \in V_h$ there exists a representation $u = \sum_{i=0}^{N} u_i$ such that*

$$a(u_0, u_0) + \sum_{i=1}^{N} a(u_i, u_i) \preceq C_0^2 a(u, u), \tag{20}$$

where $u_0 = I_0 u$, $C_0^2 \simeq \left(1 + \frac{1}{\lambda_{m+1}}\right)$ and $\lambda_{m+1} := \min\limits_{i} \min\limits_{\Gamma_{ij} \subset \partial\Omega_i} \lambda_{m_{ij}+1}^{ij}$.

Proof. Let $w := u - u_0$ and define $u_i := I_h(\theta_i w)$, where I_h is the nodal piecewise linear continuous interpolation operator on the fine mesh $\mathcal{T}_h(\Omega)$ and θ_i is a partition of unity function with respect to the partition $\{\Omega_i'\}_{i=1}^N$. θ_i is zero on $\Omega \backslash \Omega_i'$ and $\theta(x) = 1$ for $x \in \Omega_{ih}$, $\theta_i(x) = 1/2$ for $x \in \Gamma_{ijh}$, and $\theta_i(x) = 1$ when $x = x^k$.

We start by estimating $a(u_0, u_0) = \sum_{i=1}^{N} a_i(u_0, u_0)$. From the energy minimizing property of discrete harmonic functions we have for all $v \in V_h(\Omega_i)$ where $v = u_0$ on the boundary of $\partial\Omega_i$ and $v = u$ on Ω_{ih} that

$$\begin{aligned} a_i(u_0, u_0) &\leq a_i(v, v) = a_i(v - u + u, v - u + u) \\ &\leq 2a_i(v - u, v - u) + 2a_i(u, u). \end{aligned}$$

Using the fact that $u - v$ is zero on Ω_{ih} we then get

$$a_i(v - u, v - u) \preceq \sum_{\Gamma_{ij} \subset \partial\Omega_i} h_i \|u - u_0\|_{b_{\Gamma_{ij}}}^2. \tag{21}$$

By applying Lemma 2.2 we have for each edge $\Gamma_{ij} \subset \partial\Omega_i$ that

$$\begin{aligned} \|u - u_0\|_{b_{\Gamma_{ij}}}^2 &= \|(u - I_{\mathrm{ms}} u) - \Pi_{\mathrm{m}}(u - I_{\mathrm{ms}} u)\|_{b_{\Gamma_{ij}}}^2 \\ &\preceq \frac{1}{\lambda_{ij}^{m_{ij}+1}} |(u - I_{\mathrm{ms}} u) - \Pi_{\mathrm{m}}(u - I_{\mathrm{ms}} u)|_{\bar{a}_{\Gamma_{ij}}}^2 \\ &\preceq \frac{1}{\lambda_{ij}^{m_{ij}+1}} |u - I_{\mathrm{ms}} u|_{\bar{a}_{\Gamma_{ij}}}^2 \preceq \frac{1}{\lambda_{ij}^{m_{ij}+1}} |u|_{\bar{a}_{\Gamma_{ij}}}^2. \end{aligned} \tag{22}$$

The last inequality follows straightforwardly from Lemma 2.2 and the a-stability property of the 1D multiscale operator. By defining $\lambda_{m_i+1}^i := \min\limits_{\Gamma_{ij} \subset \partial\Omega_i} \lambda_{m_{ij}+1}^{ij}$ and using (4) we have that

$$\begin{aligned} \sum_{\Gamma_{ij} \subset \partial\Omega_i} \frac{h_i}{\lambda_{ij}^{m_{ij}+1}} |u|_{\bar{a}_{\Gamma_{ij}}}^2 &\simeq \sum_{\Gamma_{ij} \subset \partial\Omega_i} \frac{h_i}{\lambda_{ij}^{m_{ij}+1}} \left(|u|_{a_{\Gamma_{ij}}}^2 + |u|_{a_{\Gamma_{ji}}}^2 \right) \\ &\preceq \frac{1}{\lambda_{m_i+1}^i} \left(|u|_{a,\Omega_i^h}^2 + \sum_{\Gamma_{ij} \subset \partial\Omega_i} |u|_{a,\Omega_j^h}^2 \right) \\ &\leq \frac{1}{\lambda_{m_i+1}^i} \left(|u|_{a,\Omega_i}^2 + \sum_{\Gamma_{ij} \subset \partial\Omega_i} |u|_{a,\Omega_j}^2 \right), \end{aligned} \tag{23}$$

where in the second inequality above we extend the estimate from the boundary to the subdomain layer, while in the last inequality we extend from the subdomain layer to the whole of the subdomain. Then, by summing over each subdomain and defining $\lambda_{m+1} := \min_i \lambda^i_{m_i+1}$ completes the first part of the proof.

Now we need to provide the same type of bound for the local terms u_i, i.e.

$$\sum_{i=1}^{N} a(u_i, u_i) \preceq \frac{1}{\lambda_{m+1}} a(u, u). \tag{24}$$

Since we are only considering two layers of overlap and by adding and subtracting $u - u_0$ we have

$$\begin{aligned} a(u_i, u_i) &= a_{\Omega_i' \setminus \overline{\Omega}_i}(u_i, u_i) + a_{\Omega_i}(u_i - (u - u_0) + (u - u_0), u_i - (u - u_0) + (u - u_0)) \\ &\leq a_{\Omega_i' \setminus \overline{\Omega}_i}(u_i, u_i) + 2a_{\Omega_i}(u - u_0, u - u_0) + 2a_{\Omega_i}(u_i - (u - u_0), u_i - (u - u_0)) \\ &\simeq a_{\Omega_i}(u - u_0, u - u_0) + \sum_{\Gamma_{ij} \subset \partial\Omega_i} h_i \|u - u_0\|^2_{b_{\Gamma_{ij}}}. \end{aligned}$$

The last term in the inequality above has already been estimated so finally we have that

$$\sum_{i=0}^{N} a(u_i, u_i) \preceq \left(1 + \frac{1}{\lambda_{m+1}}\right) a(u, u), \tag{25}$$

which completes the proof of (20).

□

Remark 4.2. *The theoretical results developed in this section easily extend to the case of minimal overlap h. The only modifications needed in the proof of Lemma 4.1 are for the local components $a(u_i, u_i)$. Instead of splitting the overlapping subdomain Ω_i' into $\Omega_i' \setminus \overline{\Omega}_i$ and Ω_i, one instead splits the overlapping zone of Ω_i', i.e., the part that is shared by two or more subdomains, into the part outside of the coarse grid elements and the part that is inside the coarse grid elements and then proceed in a similar fashion as in the proof above.*

Theorem 4.3. *The condition number of the two level Schwarz operator (6) with the SHEM coarse space (16) can be bounded by*

$$\kappa(\mathbf{TA}) \preceq \omega C_0^2 (\rho(E) + 1) \tag{26}$$

where C_0 is defined as in Lemma 4.1, $\omega = 1$ and $\mathbf{TA}$ is the matrix representation of our preconditioned system.

Proof. Following the Schwarz framework, cf. [27, 29], we need to prove three assumptions:

Assumption (1)**.** *This assumption is the stable decomposition one which we have already proved in Lemma 4.1.*

Assumption (2)**.** *Let $0 \leq \mathcal{E}_{ij} \leq 1$ be the minimal values that satisfy*

$$a(u_i, u_j) \leq \mathcal{E}_{ij} a(u_i, u_i)^{1/2} a(u_j, u_j)^{1/2}, \qquad \forall u_i \in V_i,\ \forall u_j \in V_j\ i, j = 1, \ldots, N$$

Define $\rho(\mathcal{E})$ to be the spectral radius of $\mathcal{E} = \{\mathcal{E}_{ij}\}$.

Assumption (3)**.** *Let $\omega > 0$ be the minimal constant such that*

$$a(u, u) \leq \omega b_i(u, u), \qquad u \in V_i.$$

We use exact bilinear forms, i.e., $b_i(u, u) = a(u, u)$, so in our case $\omega = 1$ for $i = 1, \ldots, N$. □

5. Non-Spectral Harmonic Enrichment

Similar coarse basis functions as the ones constructed in the previous section may also be constructed without solving eigenvalue problems on the interfaces. Instead we may solve local lower dimensional problems and extend the solutions harmonically inside each subdomain in the same manner as for the eigenfunctions.

For this variant of the method we construct the basis functions by solving on each interface Γ_{ij} the 1D problem

$$\begin{aligned} \bar{a}_{\Gamma_{ij}}(\phi^k_{\Gamma_{ij}}, v) &= b_{\Gamma_{ij}}(g^k, v) \qquad \forall v \in V_h^0(\Gamma_{ij}), \\ \phi^k_{\Gamma_{ij}} &= 0 \qquad x \in \partial\Gamma_{ij}, \end{aligned} \tag{27}$$

where $b_{\Gamma_{ij}}(\cdot,\cdot)$ is given in Definition 2.1 and the alternating function g^k is defined in the following way: let $\gamma_{ij} : [0,1] \to \Gamma_{ij}$ be a parametrization of the interface Γ_{ij}, where $\gamma_{ij}(0)$ and $\gamma_{ij}(1)$ describe the end points of Γ_{ij} and let k denote the number of the basis functions used for enrichment. The alternating function $g^k(x)$ is then defined for each k by

$$g^k(\gamma_{ij}(t)) := \begin{cases} 1, & t \in [0, \frac{1}{k}], \\ -1, & t \in (\frac{1}{k}, \frac{2}{k}], \\ \vdots & \\ (-1)^{k-1}, & t \in (\frac{k-1}{k}, 1]. \end{cases}$$

Other choices for g^k are also possible: one could for instance choose g^k to be a family of sine functions or hierarchical basis functions. In any case the crucial part for achieving the same robust behavior as in the eigenfunction case is that we use the weighted L^2 inner product on the right hand side in (27).

Next, we extend these solutions harmonically inside the two subdomains sharing Γ_{ij} as an edge in the same manner as for the eigenfunctions, i.e. for each subdomain sharing Γ_{ij}, we solve

$$\begin{aligned} a_i(\chi^k_{\Gamma_{ij}}, v) &= 0 \qquad \forall v \in V_h^0(\Omega_i), \\ \chi^k_{\Gamma_{ij}} &= \phi^k_{\Gamma_{ij}} \quad x \in \Gamma_{ij}, \\ \chi^k_{\Gamma_{ij}} &= 0 \qquad x \in (\partial\Omega_i \cup \partial\Omega_j) \setminus \Gamma_{ij}, \end{aligned} \tag{28}$$

and extend the solution with zero to the rest of Ω.

The non-spectral harmonically enriched multiscale coarse space (NSHEM) is then defined as the span of the two sets of basis functions

$$V_0^* := \text{span}\{\{\phi_k^{ms}\}_{k=1}^{n_\nu} \cup \{\{\chi^l_{\Gamma_{ij}}\}_{l=1}^{m_{ij}}\}_{\Gamma_{ij}\subset\Gamma}. \tag{29}$$

We will also refer to the above basis functions as non-spectral functions. An example of such functions for $k = 1$ and $k = 2$ are given in Figure 4 for a problem with $\alpha = 1$ and mesh parameters $H = 1/2$ and $h = 1/32$. We see a close resemblance to the spectral basis functions given in Figure 3 and in the next section we show with numerical examples that the behavior for these variants of the coarse enrichment is almost identical to the behavior of the eigenfunction variant.

6. Numerical Results

We now present extensive numerical experiments for the new coarse spaces solving problem (1) on a unit square domain, i.e. $\Omega = (0,1)^2$, where the right hand side is chosen to be $f = 1$,

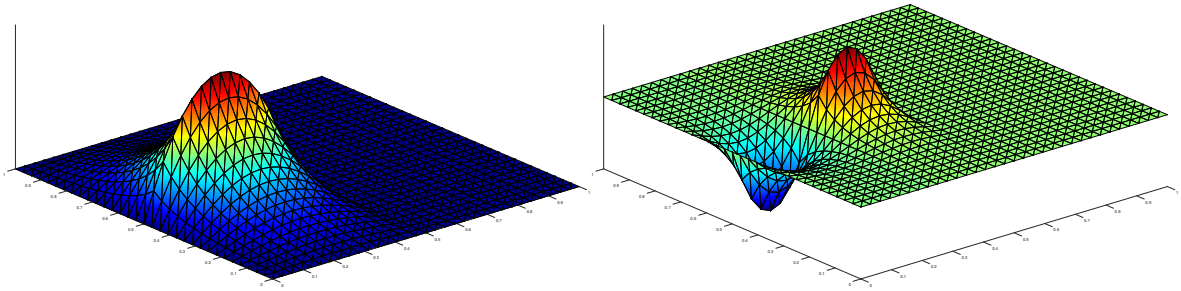

FIGURE 4. Plot of the non-spectral basis functions for $h = 1/32$ and $H = 16h$. *Left:* first order non-spectral basis functions. *Right:* second order non-spectral basis functions.

Type:	SHEM_3	NSHEM_3^a	NSHEM_3^s	NSHEM_3^h
$\hat{\alpha}$	#it. (κ)	#it. (κ)	#it. (κ)	#it. (κ)
10^0	13 (5.19e0)	13 (5.50e0)	13 (5.19e0)	17 (8.26e0)
10^2	18 (7.42e0)	19 (7.74e0)	19 (7.80e0)	20 (7.58e0)
10^4	19 (7.44e0)	19 (7.49e0)	19 (7.44e0)	20 (7.60e0)
10^6	19 (7.44e0)	19 (7.49e0)	19 (7.44e0)	21 (7.61e0)

TABLE 2. Comparison of the iteration count and condition number estimate for SHEM_3 and the three NSHEM_3 variants for the distribution given in Figure 5 with $h = \frac{1}{128}$, $H = 16h$.

and the coefficient $\alpha(x)$ represents various (possibly discontinuous) distributions. We test the new coarse spaces with the two level additive Schwarz (AS) method, where the coarse spaces have been enriched with different numbers of spectral and non-spectral basis functions on each interface, and then AS is used as a preconditioner for the conjugate gradient method. For all numerical examples, we run the preconditioned conjugate gradient method until the l_2 norm of the initial residual is reduced by a factor of 10^6, that is, until $\|r_i\|_2/\|r_0\|_2 \leq 10^{-6}$. The coefficient $\alpha(x)$ for all the numerical examples is equal to 1, except in the areas marked with red where the value of $\alpha(x)$ is equal to $\hat{\alpha}$.

6.1. **Comparison of SHEM and NSHEM.** We start by showing that SHEM and the three variants of NSHEM introduced in the previous sections have similar performance. To do so, we use the distribution of α with three inclusions of different size crossing interfaces between subdomains in Figure 5. We test the case where the multiscale coarse space is enriched with three basis functions on each interface (SHEM_3) and compare the number of iterations and condition number in Table 2 to NSHEM_3^a, which denotes the variant with three piecewise constant alternating function g^k in the definition (27), NSHEM_3^s, which uses sine functions for g^k, and NSHEM_3^h, which uses hierarchical basis functions for g^k. We see from the results in Table 2 that the performance of the four variants is very similar. In fact, for the first three variants of the coarse enrichment, the performance of the method is basically identical.

We next revisit the distribution of α given in Figure 1, and compare SHEM_i and NSHEM_i^a with a varying number of basis functions $i = 1, 2, 3, 4$ on each interface. We state the number

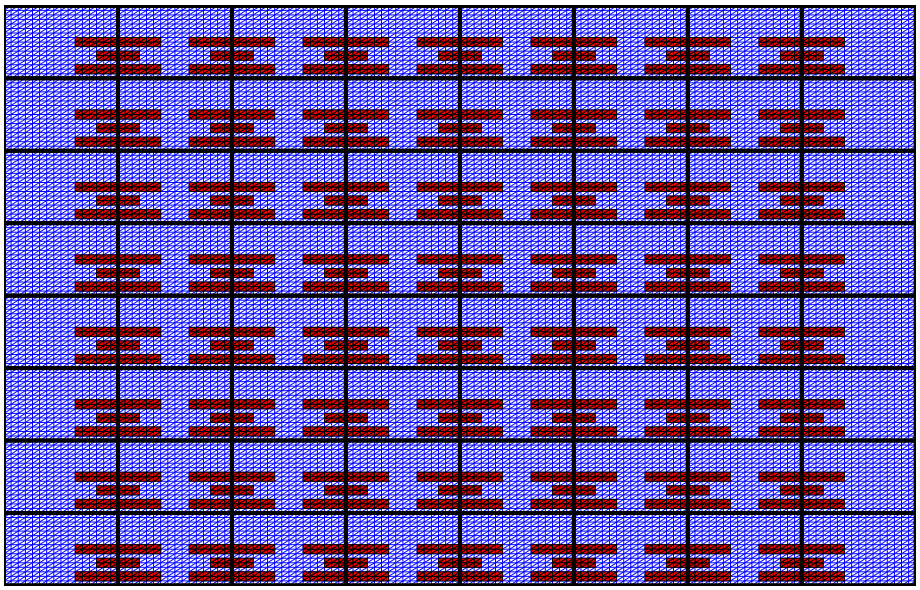

FIGURE 5. Distribution of α for a geometry with $h = \frac{1}{128}$, $H = 16h$. The regions marked with red are where α has a large value.

	MS	SHEM_1	SHEM_2	SHEM_3	SHEM_4
dim.	49	161	273	385	497
$\hat{\alpha}$	#it. (κ)	#it. (κ)	#it. (κ)	#it. (κ)	#it. (κ)
10^0	21 (1.29e1)	16 (7.45e0)	15 (5.99e0)	13 (5.19e0)	13 (5.15e0)
10^2	122 (3.74e2)	70 (1.17e2)	47 (6.70e1)	19 (6.77e0)	16 (5.66e0)
10^4	367 (3.64e4)	248 (1.10e4)	187 (6.22e3)	19 (6.78e0)	17 (5.73e0)
10^6	610 (3.64e6)	423 (1.10e6)	290 (6.22e5)	19 (6.78e0)	17 (5.73e0)

TABLE 3. Iteration count and condition number estimate for the distribution in Figure 1 for the classical multiscale coarse space (MS) and different numbers of spectral basis functions $i = 1, 2, 3, 4$ in SHEM_i with $h = \frac{1}{128}$, $H = 16h$.

of iterations and condition number for each run in the Table 3 and 4. We see again that the performance of SHEM_i and NSHEM_i^a is very similar, and the solver becomes robust for the same number $i = 3$ of enrichment functions, corresponding to the number of inclusions across the interfaces.

6.2. **An Adaptive Variant of SHEM.** In Table 5 we give the number of iterations and condition number for an adaptive version we call $\text{SHEM}_{\text{adapt}}$ in the case of the distribution of α given in Figure 1: on each interface shared by two subdomains we enrich the coarse space with spectral basis functions corresponding to eigenvalues below a certain threshold. By comparing the eigenvalues to the eigenvalues of the Laplacian we may choose the threshold in such a way that we only include spectral functions corresponding to eigenvalues that are

	NSHEM_1^a	NSHEM_2^a	NSHEM_3^a	NSHEM_4^a
dim.	161	273	385	497
$\hat{\alpha}$	#it. (κ)	#it. (κ)	#it. (κ)	#it. (κ)
10^0	16 (7.52e0)	14 (6.06e0)	13 (5.50e0)	13 (5.23e0)
10^2	71 (1.17e2)	49 (6.92e1)	19 (6.79e0)	17 (5.74e0)
10^4	256 (1.11e4)	130 (6.45e3)	20 (6.81e0)	20 (6.67e0)
10^6	454 (1.11e6)	221 (6.45e5)	20 (6.81e0)	20 (6.67e0)

TABLE 4. Iteration count and condition number estimate for the distribution in Figure 1 for different numbers of non-spectral basis functions $i = 1, 2, 3, 4$ in NSHEM_i^a with $h = \frac{1}{128}$, $H = 16h$.

$\text{SHEM}_{\text{adapt}}$		
$\hat{\alpha}$	#it. (κ)	dim.
10^0	21 (1.29e1)	49
10^2	25 (1.10e1)	233
10^4	25 (1.09e1)	233
10^6	25 (1.09e1)	233

TABLE 5. Iteration and condition number estimate for the distribution in Figure 1 for $\text{SHEM}_{\text{adapt}}$ with $h = \frac{1}{128}$, $H = 16h$.

	non-overlapping	overlapping
$\hat{\alpha}$	#it. (κ)	#it. (κ)
10^0	1 (1)	10 (5)
10^2	1 (1)	13 (5)
10^4	1 (1)	13 (5)
10^6	1 (1)	13 (5)

TABLE 6. Iteration and condition number estimate for OHEM applied to the distribution in Figure 1 with $h = \frac{1}{128}$, $H = 16h$.

smaller than the smallest eigenvalue of the Laplacian on each interface. Eigenvalues below this threshold will correspond to discontinuities along the subdomain boundaries.

By studying the dimension of the enriched coarse space in Table 5 we see that by a proper choice of the cut-off criteria the method is completely insensitive to any discontinuity inside subdomains and along subdomain boundaries. Also, if we count the number of high conducting regions in Figure 1 crossing the interfaces, we see that the number of eigenfunctions needed on each interface equals the number of inclusions or channels crossing it.

6.3. **An Example of OHEM.** If all of the spectral basis functions corresponding to each interface are included, then the coarse space spans the full discrete harmonic function space $\tilde{V}_h$, which is the optimal harmonically enriched multiscale coarse space (OHEM), and the method can be made into a direct solver: The subdomain solves are only used to incorporate the influence of the right hand side function into the solution, while the full harmonic space then connects and shifts them correctly, and overlap is not needed any more. In Table 6, we show some numerical results for the non-overlapping case, where we obtain the solution in one iteration, and the corresponding overlapping method, where we see that the error the additive Schwarz method commits in the overlap to remain symmetric (see [8, 12]) prevents the method from converging in one iteration. This can be corrected using RAS which will be

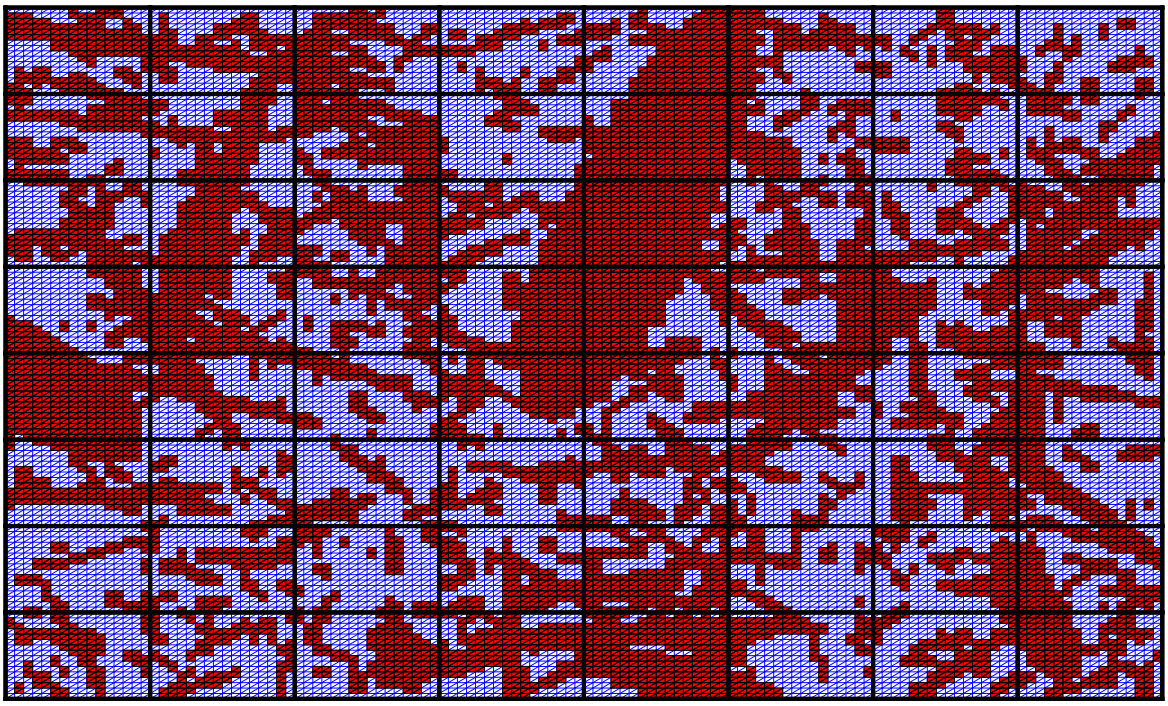

FIGURE 6. Distribution of α for a geometry with $h = \frac{1}{128}$, $H = 16h$. The regions marked with red are where α has a large value.

Type:	SHEM_3		$\text{SHEM}_{\text{adapt}}$	
$\hat{\alpha}$	#it. (κ)	dim.	#it. (κ)	dim.
10^0	13 (5.19e0)	385	16 (7.45e0)	161
10^2	22 (9.47e0)	385	25 (1.07e1)	239
10^4	23 (9.60e0)	385	26 (1.11e1)	236
10^6	24 (9.59e0)	385	28 (1.08e1)	236

TABLE 7. Iteration and condition number estimate for the distribution in Figure 6 comparing SHEM_3 and $\text{SHEM}_{\text{adapt}}$ with $h = \frac{1}{128}$, $H = 16h$.

shown in [16], see also [14]. OHEM is not really a practical method, since the coarse space is very big, but it is of great theoretical interest, since it defines precisely which object a good coarse space should approximate, and this is how we discovered SHEM and NSHEM, see also [15] where this complete coarse space information is encoded in transmission conditions between subdomains.

6.4. **Highly Irregular Conductivities and Subdomains.** We now test the case where we allow the distribution of α to be highly irregular. Inspired by an example in [30] we consider a slightly modified version of it, as depicted in Figure 6. For this case we choose the threshold for the adaptive variant $\text{SHEM}_{\text{adapt}}$ in such a way that we are guaranteed at least one spectral basis function on each edge. The number of iterations and condition numbers for increasing $\hat{\alpha}$ are given in Table 7 for SHEM_3 and $\text{SHEM}_{\text{adapt}}$. We see from the table that the dimension of the coarse space is still lower than the dimension for the local subspaces. In addition,

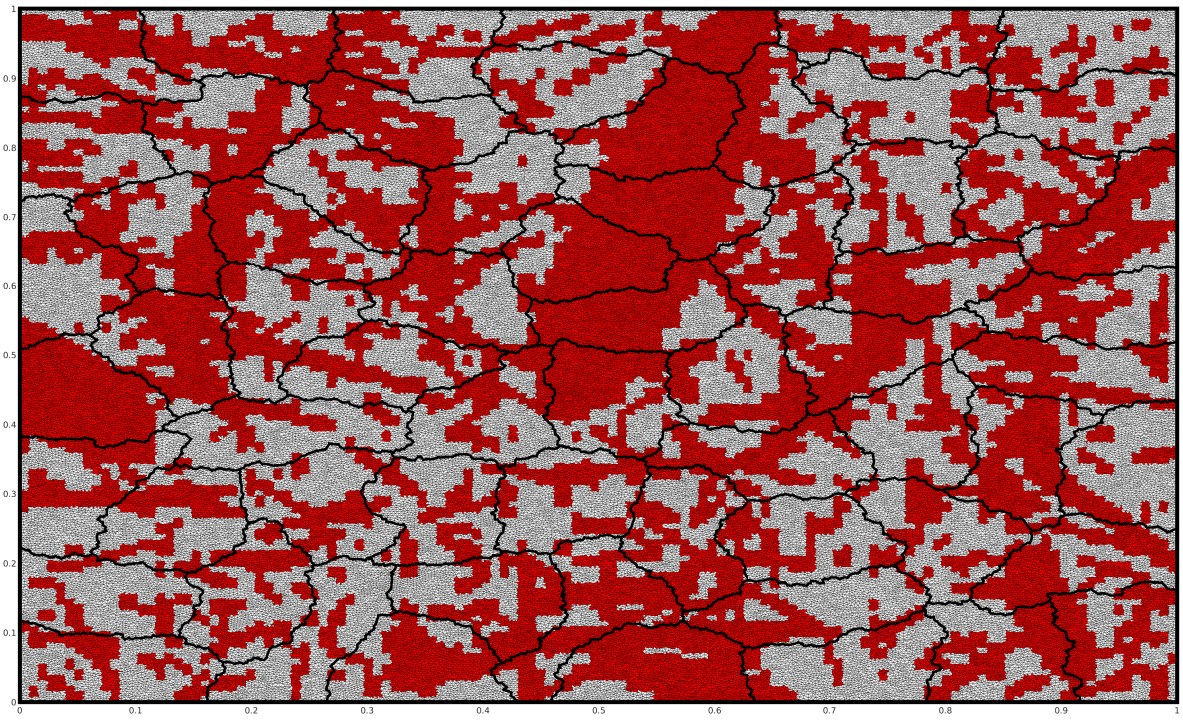

FIGURE 7. Distribution of α for a geometry discretized with 226918 irregular triangles and partitioned into 64 irregular subdomains with METIS. The regions marked with red are where α has a large value. The largest subdomain has 1889 dofs.

we see that the performance of $\text{SHEM}_{\text{adapt}}$ with a substantially smaller coarse space is still comparable to SHEM_3 with three enrichment functions on each interface.

In order to test SHEM on more realistic problems, we consider now the case where Ω is subdivided into irregular fine triangles for the fine mesh and irregular subdomains arising from the graph partitioning software METIS [19] for the subdomains and the coarse mesh. For these experiments, we consider only the adaptive variant $\text{SHEM}_{\text{adapt}}$ and compare it with the standard multiscale coarse space without enrichment we denote by MS. For our first example, we modify the distribution given in Figure 6 by discretizing it with an irregular mesh such that the largest diameter of the elements is $1/256$. We then partition the mesh into irregular subdomains using METIS, see Figure 7. The tolerance for including spectral functions into the coarse space is set to $\tau = 1/32$ and the iteration count and condition number estimate for `pcg` are given in Table 8 where we also report the size of the coarse space. For the second example, we consider the same fine grid and coarse grid as in the previous example, but now the coefficients α are taken as the permeability field from the bottom layer of the SPE 10th comparative solution project [3], see Figure 8. We compare the results of MS with $\text{SHEM}_{\text{adapt}}$ for three different choices of the tolerance τ and report the iteration count and condition number estimate for `pcg` in Table 8 in addition to the number of coarse basis functions for each choice of τ. These examples show that $\text{SHEM}_{\text{adapt}}$ performs very well even for very hard problems and much better than MS that only uses the initial multiscale coarse space. For all choices of the tolerance τ, the $\text{SHEM}_{\text{adapt}}$ is insensitive to the irregularities of both the

Type:	MS		$\text{SHEM}_{\text{adapt}}$	
$\hat{\alpha}$	#it. (κ)	dim.	#it. (κ)	dim.
10^0	47 (3.55e1)	101	21 (6.95e0)	676
10^2	143 (7.49e2)	101	28 (1.11e1)	738
10^4	699 (3.50e4)	101	28 (1.10e1)	738
10^6	898 (3.41e6)*	101	30 (1.10e1)	738

* Stagnation.

TABLE 8. Comparison of the iteration count and condition number estimate for MS (without enrichment) and $\text{SHEM}_{\text{adapt}}$ with tolerance $\tau = 1/32$ for the problem given in Figure 7. The number of coarse dofs for both methods is given in the columns next to the iteration count and condition number estimate.

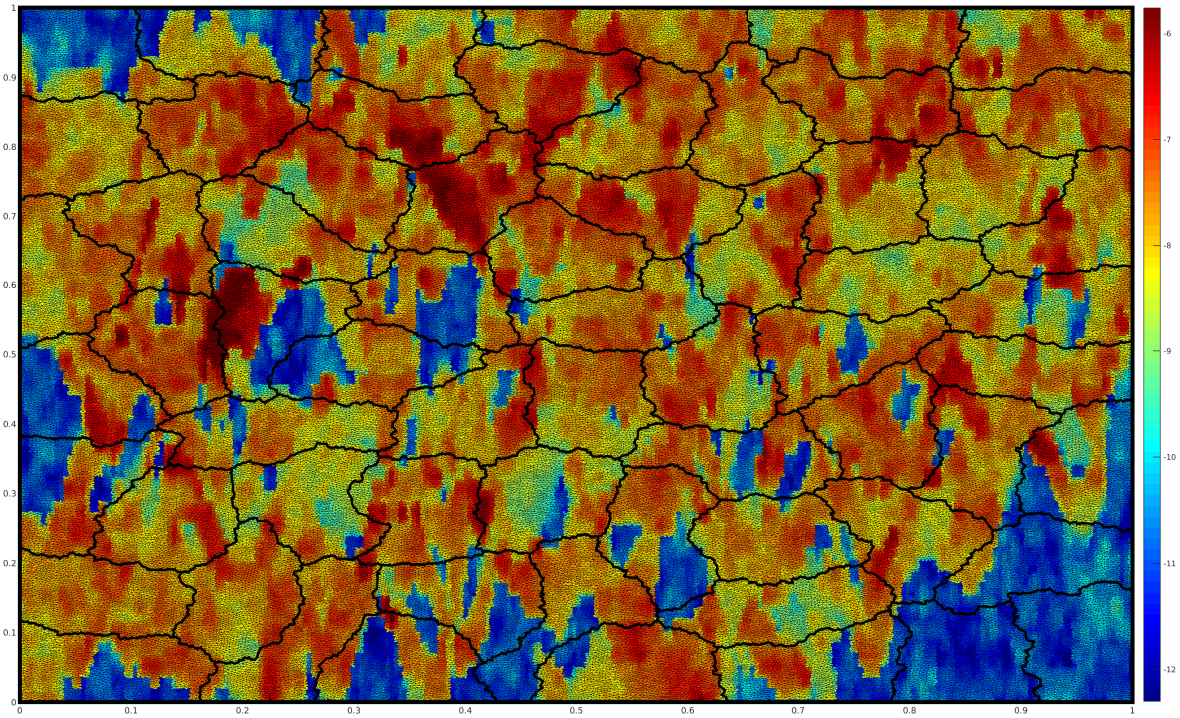

FIGURE 8. Base 10 logarithm of the permeability field corresponding to the SPE10 Bottom Layer test case for a geometry discretized with 226918 irregular triangles and partitioned into 64 irregular subdomains with METIS. The largest subdomain has 1889 dofs.

subdomain/coarse partitioning and the fine grid and also with respect to the high contrast in the underlying material coefficient, without the dimension of the coarse space becoming larger than the dimension of the largest subdomain and thus the coarse solve never becomes the bottleneck of the method.

Type:	MS		$\text{SHEM}_{\text{adapt}}$	
τ	#it. (κ)	dim.	#it. (κ)	dim.
$\frac{1}{64}$	124 (3.75e2)	101	30 (1.23e1)	489
$\frac{1}{32}$	124 (3.75e2)	101	27 (1.09e1)	646
$\frac{1}{16}$	124 (3.75e2)	101	23 (7.72e0)	910

TABLE 9. Comparison of the iteration count and condition number estimate for MS (without enrichment) and $\text{SHEM}_{\text{adapt}}$ for the problem given in Figure 8. The number of coarse dofs for both methods is given in the columns next to the iteration count and condition number estimate.

7. Conclusion

We introduced a new harmonically enriched multiscale coarse space (HEM) based on the multiscale coarse space from [17]. Our first enrichment process uses lower dimensional eigenvalue problems on interfaces between subdomains and extends these solutions harmonically inside each of the corresponding subdomains sharing the interface, which leads to the spectral harmonically enriched multiscale coarse space (SHEM). We showed both theoretically and numerically that SHEM guarantees robustness with respect to the discontinuities/variations of the coefficient in the problem. When we complete the enrichment to the full discrete harmonic space, the coarse space becomes optimal (OHEM) and the method turns into a direct solver.

We then proposed three enrichment variants not based on eigenvalue problems (NSHEM), which simply solve lower dimensional variants of the original problem on the interfaces between subdomains. Our numerical experiments showed that NSHEM performs equally well in practice as SHEM. NSHEM does however not have the eigenvalue information that can be used as a natural measure to make NSHEM into an adaptive method that guarantees robustness with respect to the contrast.

The new coarse spaces based on harmonic enrichment are not only excellent coarse spaces for the high contrast elliptic model problem we considered, they are also an ideal choice for many other partial differential equations, since they are based on the approximation of an optimal coarse space which contains all coarse space components necessary to turn the domain decomposition method into a direct solver.

Acknowledgment

We thank Professor Leszek Marcinkowski for his comments, particularly for pointing out to us that Definition 2.1 in our earlier version did not cover the case where elements with large coefficients would touch subdomain boundaries at only one point.

References

[1] Jørg Aarnes and Thomas Y. Hou. Multiscale domain decomposition methods for elliptic problems with high aspect ratios. *Acta Math. Appl. Sin. Engl. Ser.*, 18(1):63–76, 2002.

[2] Petter E. Bjørstad, Maksymilian Dryja, and Eero Vainikko. Additive Schwarz methods without subdomain overlap and with new coarse spaces. In *Domain decomposition methods in sciences and engineering (Beijing, 1995)*, pages 141–157. Wiley, Chichester, 1997.

[3] MA Christie, MJ Blunt, et al. Tenth spe comparative solution project: A comparison of upscaling techniques. In *SPE Reservoir Simulation Symposium*. Society of Petroleum Engineers, 2001.

[4] Victorita Dolean, Frédéric Nataf, Robert Scheichl, and Nicole Spillane. Analysis of a two-level Schwarz method with coarse spaces based on local Dirichlet-to-Neumann maps. *Comput. Methods Appl. Math.*, 12(4):391–414, 2012.

[5] Maksymilian Dryja, Marcus V. Sarkis, and Olof B. Widlund. Multilevel Schwarz methods for elliptic problems with discontinuous coefficients in three dimensions. *Numer. Math.*, 72(3):313–348, 1996.
[6] Maksymilian Dryja, Barry F. Smith, and Olof B. Widlund. Schwarz analysis of iterative substructuring algorithms for elliptic problems in three dimensions. *SIAM J. Numer. Anal.*, 31(6):1662–1694, 1994.
[7] Yalchin Efendiev, Juan Galvis, Raytcho Lazarov, and Joerg Willems. Robust domain decomposition preconditioners for abstract symmetric positive definite bilinear forms. *ESAIM Math. Model. Numer. Anal.*, 46(5):1175–1199, 2012.
[8] Evridiki Efstathiou and Martin J. Gander. Why restricted additive Schwarz converges faster than additive Schwarz. *BIT*, 43(suppl.):945–959, 2003.
[9] Juan Galvis and Yalchin Efendiev. Domain decomposition preconditioners for multiscale flows in high-contrast media. *Multiscale Model. Simul.*, 8(4):1461–1483, 2010.
[10] Juan Galvis and Yalchin Efendiev. Domain decomposition preconditioners for multiscale flows in high contrast media: reduced dimension coarse spaces. *Multiscale Model. Simul.*, 8(5):1621–1644, 2010.
[11] Martin J. Gander. Optimized Schwarz methods. *SIAM J. Numer. Anal.*, 44(2):699–731, 2006.
[12] Martin J. Gander. Schwarz methods over the course of time. *Electron. Trans. Numer. Anal.*, 31:228–255, 2008.
[13] Martin J. Gander, Laurence Halpern, and Kévin Santugini. Discontinuous coarse spaces for DD-methods with discontinuous iterates. In *Domain Decomposition Methods in Science and Engineering XXI. Springer LNCSE*. Springer, 2014.
[14] Martin J. Gander, Laurence Halpern, and Kévin Santugini. A new coarse grid correction for RAS/AS. In *Domain Decomposition Methods in Science and Engineering XXI. Springer LNCSE*. Springer, 2014.
[15] Martin J Gander and Felix Kwok. Optimal interface conditions for an arbitrary decomposition into subdomains. In *Domain Decomposition Methods in Science and Engineering XIX*, pages 101–108. Springer, 2011.
[16] Martin J. Gander and Atle Loneland. An optimal coarse space for RAS and its multiscale approximation. In *In Preperation*. 2016.
[17] I. G. Graham, P. O. Lechner, and R. Scheichl. Domain decomposition for multiscale PDEs. *Numer. Math.*, 106(4):589–626, 2007.
[18] Thomas Y. Hou and Xiao-Hui Wu. A multiscale finite element method for elliptic problems in composite materials and porous media. *J. Comput. Phys.*, 134(1):169–189, 1997.
[19] George Karypis and Vipin Kumar. A fast and high quality multilevel scheme for partitioning irregular graphs. *SIAM Journal on Scientific Computing*, 20(1):359–392, 1998.
[20] Jan Mandel and Marian Brezina. Balancing domain decomposition for problems with large jumps in coefficients. *Math. Comp.*, 65(216):1387–1401, 1996.
[21] Fréderíc Nataf and Francois Rogier. Factorization of the convection-diffusion operator and the Schwarz algorithm. M^3AS, 5(1):67–93, 1995.
[22] J. M. Nordbotten and P. E. Bjørstad. On the relationship between the multiscale finite-volume method and domain decomposition preconditioners. *Comput. Geosci.*, 12(3):367–376, 2008.
[23] Clemens Pechstein and Robert Scheichl. Analysis of FETI methods for multiscale PDEs. *Numer. Math.*, 111(2):293–333, 2008.
[24] Clemens Pechstein and Robert Scheichl. Analysis of FETI methods for multiscale PDEs. Part II: interface variation. *Numer. Math.*, 118(3):485–529, 2011.
[25] Marcus Sarkis. Nonstandard coarse spaces and Schwarz methods for elliptic problems with discontinuous coefficients using non-conforming elements. *Numer. Math.*, 77(3):383–406, 1997.
[26] Robert Scheichl. Robust coarsening in multiscale pdes. In Randolph Bank, Michael Holst, Olof Widlund, and Jinchao Xu, editors, *Domain Decomposition Methods in Science and Engineering XX*, volume 91 of *Lecture Notes in Computational Science and Engineering*, pages 51–62. Springer Berlin Heidelberg, 2013.
[27] Barry Smith, Petter Bjorstad, and William Gropp. *Domain decomposition: parallel multilevel methods for elliptic partial differential equations*. Cambridge University Press, 1996.
[28] N. Spillane, V. Dolean, P. Hauret, F. Nataf, C. Pechstein, and R. Scheichl. Abstract robust coarse spaces for systems of PDEs via generalized eigenproblems in the overlaps. *Numer. Math.*, 126(4):741–770, 2014.
[29] Andrea Toselli and Olof Widlund. *Domain decomposition methods—algorithms and theory*, volume 34 of *Springer Series in Computational Mathematics*. Springer-Verlag, Berlin, 2005.

[30] J. Willems. Spectral coarse spaces in robust two-level Schwarz methods. In *Numerical solution of partial differential equations: theory, algorithms, and their applications*, volume 45 of *Springer Proc. Math. Stat.*, pages 303–326. Springer, New York, 2013.
[31] Jinchao Xu and Jun Zou. Some nonoverlapping domain decomposition methods. *SIAM Rev.*, 40(4):857–914, 1998.

Section of Mathematics, University of Geneva, 1211 Geneva 4, Switzerland
E-mail address: Martin.Gander@unige.ch

Department of Informatics, University of Bergen, 5020 Bergen, Norway
E-mail address: Atle.Loneland@ii.uib.no

Department of Computing, Mathematics and Physics, Bergen University College, 5020 Bergen, Norway
E-mail address: Talal.Rahman@hib.no